Ground-state phases of the spin-orbit-coupled spin-1 Bose gas in a toroidal trap

Ji-Guo Wang,[1,2] Liang-Liang Xu,[2] and Shi-Jie Yang[2,*]
[1]*Department of Mathematics and Physics, Shijiazhuang TieDao University, Shijiazhuang 050043, China*
[2]*Department of Physics, Beijing Normal University, Beijing 100875, China*
(Received 30 June 2017; published 25 September 2017)

We consider the spin-1 Bose-Einstein condensates with the isotropic Rashba spin-orbit coupling in a two-dimensional toroidal trap. Three types of striped phases are found in a nonrotational system, i.e., the stripe phase with the periodic density modulation along the azimuthal direction, the stripe phase with the periodic density modulation along both the azimuthal and the radial directions, and the stripe phase with the periodic density modulation along the radial direction. By adding the rotation, the condensates occupy the $m_F = 0$ component for small rotational frequency, while they occupy both the $m_F = 1$ and $m_F = -1$ components for large rotational frequency when both the relative interaction and the spin-orbit coupling are weak. For the stronger relative interaction and spin-orbit coupling, the vortices of the system are elongated along the radial direction and linked one after another. As the rotational frequency further increases, the density evolves from the elongated effect of the vortices into a laminar vortex ring.

DOI: 10.1103/PhysRevA.96.033629

I. INTRODUCTION

The spin-orbit coupling (SOC) plays an important role in many branches of physics, such as the quantum spin Hall effect and topological insulators [1–5]. The experimental progress of the SOC in the spin-1/2 Bose-Einstein condensate (BEC) and the Fermi gases has attracted great attention [6–11]. Many new phases have emerged due to the SOC, such as the stripe phase [12,13] in the homogenous BEC, half-quantum vortex configuration [14–17] in the trapped BEC, and the topological superfluidity [18] for fermions. When combining both the SOC and the rotation in the BEC system with a harmonic trap, various novel features have been predicted to occur [19–23]. Inspired by the experimental schemes of the SOC in ultracold atoms by employing an optical field to couple internal states or using gradient magnetic fields [24–30], a rich variety of works about the spin-orbit-coupled spin-1 BEC have been studied [31–38], in which nontrivial ground-state phases are predicted.

The toroidal trap can be realized by a blue-detuned laser beam to make a repulsive potential barrier in the middle of a harmonic magnetic trap [39]. BEC in the toroidal trap is used to study the persistent currents, formation of matter-wave patterns by rotating potentials, and solitary waves [40–43], in both experiments and theories. The spin-1/2 BEC with the SOC loaded in a two-dimensional (2D) toroidal trap [44–46] has attracted considerable interest, due to the stable necklacelike states and the persistent flow states that are found.

In this paper, we consider a spin-orbit-coupled spin-1 BEC trapped in a 2D toroidal trap. Three types of striped phases, namely, the periodically modulated stripe phase along the azimuthal direction, the periodically modulated stripe phase along both the azimuthal and the radial directions, as well as the periodically modulated stripe phase along the radial direction, are found in the nonrotational potential. For these phases, the directions of the phase gradients of the $m_F = 1$ and $m_F = -1$ components are antisymmetric. In the presence of rotation, the condensates occupy the $m_F = 0$ component for small rotational frequency, while they occupy both the $m_F = 1$ and $m_F = -1$ components for large rotational frequency, given that both the relative interaction and the SOC are weak. For strong relative interaction and SOC, the vortices of the system are elongated along the radial direction and linked one after another; with the rotation frequency increases, the density evolves from the elongated effect of the vortices into a laminar vortex ring.

The paper is organized as follows: In Sec. II, we introduce the model of the spin-orbit-coupled spin-1 Bose gas in a 2D toroidal trap. In Sec. III, we display the phase diagrams without rotation. In Sec. IV, a variety of ground-state phase structures is found for the rotating condensates. A summary is included in Sec. V.

II. MODEL

We consider the spin-1 BEC with isotropic Rashba SOC trapped in a 2D toroidal trap. The Hamiltonian of the system is given by $H = H_0 + H_{\rm int}$, where

$$H_0 = \int d\mathbf{r}\Psi_j^\dagger\Big[-\frac{\hbar^2}{2m_B}\nabla^2 + V(r) + \upsilon_{\rm soc} + q\left(F_x^2 + F_y^2\right) - \Omega L_z\Big]\Psi_j,$$
$$H_{\rm int} = \int d\mathbf{r}\left(\frac{1}{2}c_0 n^2 + \frac{1}{2}c_2|\mathbf{F}|^2\right), \quad (1)$$

where $\Psi_j (j = 0, \pm 1)$ is the three-component spinor wave function of the atoms condensed in the spin state $|F = 1, m_F = j\rangle$. m_B is the atomic mass, $n = n_1 + n_0 + n_{-1} = \sum_j |\psi_j|^2$ is the total density, and $\mathbf{r} = (x, y)$. The interaction strengths $c_0 = \frac{4}{3}\hbar^2\pi(2a_2 + a_0)/m_B$ and $c_2 = \frac{4}{3}\hbar^2\pi(a_2 - a_0)/m_B$ are given in terms of the s-wave scattering length a_s for atom pairs with total spin F. $\mathbf{F}$ is the spin density, $\mathbf{F} = (F_x, F_y, F_z) = (\Psi^\dagger\hat{F}_x\Psi, \Psi^\dagger\hat{F}_y\Psi, \Psi^\dagger\hat{F}_z\Psi)$, with the 3×3 spin-1 matrices $\widehat{F}$. The isotropic Rashba SOC is $\upsilon_{\rm soc} = -i\hbar\lambda(F_x\partial_y - F_y\partial_x)$ with the SOC strength λ. q is the quadratic Zeeman shift. The

*Corresponding author: yangshijie@tsinghua.org.cn

toroidal trap potential can be described by a shifted harmonic oscillator, i.e., $V(r) = \frac{1}{2}m_B\omega_r^2(r - r_0)^2$, where $r^2 = x^2 + y^2$, r_0 is the toroidal trap radius, and ω_r is the harmonic trapping frequency. The rotational frequency Ω is along the z direction with the orbit angular momentum $L_z = -i\hbar(x\partial_y - y\partial_x)$. We assume the relative interaction strength $g = c_0/c_2$ in the present paper.

In the absence of rotation ($\Omega = 0$), the wave function can be written as $\Psi(r,\phi) = R(r)\psi(\phi)$, where $R(r)$ and $\psi(\phi)$ are the wave functions along the radial direction r and the azimuthal direction (the azimuthal angle ϕ), respectively. The single-particle Hamiltonian H_0 can be rewritten as [47]

$$H_0(r,\phi) = -\frac{\hbar^2}{2m_B}\left[\frac{\partial^2}{\partial r^2} + \frac{1}{r}\frac{\partial}{\partial r} - \frac{1}{r^2}\left(i\frac{\partial}{\partial\phi}\right)^2\right] - \frac{\lambda}{r}(\cos\phi F_x + \sin\phi F_y)\left(i\frac{\partial}{\partial\phi}\right) + i\lambda(\cos\phi F_y + \sin\phi F_x)\frac{\partial}{\partial r} + V(r), \quad (2)$$

where $x = r\cos\phi$ and $y = r\sin\phi$. We can obtain the correct form of the single-particle Hamiltonian in a toroidal trap with the Rashba SOC when the toroidal trap radius is r_0,

$$H_0(\phi) = \frac{\hbar^2}{2m_B r_0^2}\left(i\frac{\partial}{\partial\phi}\right)^2 - \frac{\lambda}{r_0}(\cos\phi F_x + \sin\phi F_y) \times\left(i\frac{\partial}{\partial\phi}\right) - i\frac{\lambda}{2r_0}(\cos\phi F_y + \sin\phi F_x). \quad (3)$$

III. GROUND-STATE PHASE DIAGRAMS WITHOUT THE ROTATION

We implement the mean-field approximation to study the ground-state phases of the spin-orbit-coupled spin-1 BEC loaded in a 2D toroidal trap. To highlight the effect of the SOC and the relative interaction, we fix the toroidal trap radius $r_0 = 4$. Figure 1(a) gives the ground-state phase diagram spanned by the SOC strength λ and the relative interaction strength g without the quadratic Zeeman shift ($q = 0$). We also study the influence of the quadratic Zeeman shift ($q = 1$) on the ground state in Fig. 1(c). We note that all six phases are presented in both cases and the quadratic Zeeman term only shifts the boundaries of the phases. The quadratic Zeeman term does not change the general features of the system qualitatively. For clearance, we will not take account of the quadratic Zeeman term in the following sections.

The density and the phase profiles of the six different phases (A)–(F) in Figs. 1(a) and 1(c) are shown in Figs. 2(a)–2(f), respectively. We start from the case where the SOC is weak, which is indicated by the red region (A) in Figs. 1(a) and 1(c). In this phase, the densities of the three components are a uniform distribution around the toroidal trap, respectively, as shown in Fig. 2(a). The $m_F = 1$ and $m_F = -1$ components have the same density profiles; their density values are smaller (larger) than the $m_F = 0$ component without the quadratic Zeeman shift (with the quadratic Zeeman shift), but the density radius are larger. The winding number of the $m_F = 0$ component is zero and there exists one winding number difference compared with the $m_F = 1$ and $m_F = -1$

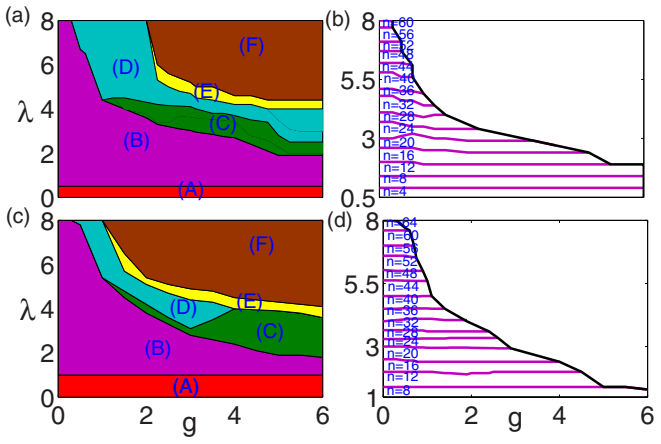

FIG. 1. The ground-state phase diagram of the nonrotational system spanned by the SOC strength λ and the relative interaction strength g for (a) without the quadratic Zeeman shift ($q = 0$) and (c) with the quadratic Zeeman shift ($q = 1$). The six phases are marked by (A)–(F). The toroidal trap radius $r_0 = 4$. (b) and (d) are the details of the phase structures of the (B) phase in (a) and (c), respectively. The number of the petals $n = 4l$, with l an integer number.

components. For the fixed value of r_0, the boundary of the (A) phase is independent of g. As the SOC is increased to $\lambda = 0.5$ ($\lambda = 1.0$) without the quadratic Zeeman shift (with the quadratic Zeeman shift), the (A) phase transforms to the (B) phase, as shown in Fig. 1(a) [Fig. 1(c)].

We observe the exotic properties of the ground state with increasing the SOC strength λ. The (B) phase has the periodic density modulation along the azimuthal direction; it is a necklacelike state. The number of petals of the three components are the same, as shown in Fig. 2(b). This phase occupies the largest ranges of λ and g. In the limit of strong SOC but weak relative interaction, the system only has the (B) phase. In order to understand the change of the number of the petals, Figs. 1(b) and 1(d) display the detailed structures of the (B) phase without and with the quadratic Zeeman shift, respectively. We find that the number of the petals increases as the SOC strength is enhanced. The corresponding region becomes small. The number of the petals $n = 4l$, where l is an integer, and the winding number of the $m_F = 1$ and $m_F = -1$ components is $n/2 + 1$, which is different from the two-component SOC BECs [46]. For this phase, the total density [the fourth column in Fig. 2(b)] also has the periodic density modulation along the azimuthal direction.

As the SOC is further increased, the (B) phase transforms to the (D) phase for $g < 1$ and the (C) phase transforms to the (D) phase for $g \geqslant 1$, as shown in Figs. 1(a) and 1(c). The (C) phase is bent near the central hole in the half of the perimeter and tends to be perpendicular to the hole with outward expansion. The total density of the (C) phase is divided into two parts and the (D) phase is divided into four parts, as shown in Figs. 2(c) and 2(d), respectively. The (C) phase only exists in the regime of the intermediate interaction strength ($g \geqslant 1$) with or without the quadratic Zeeman shift. The regime of the (D) phase is replaced by the (C) phase in the presence of the quadratic Zeeman shift and with strong relative interaction. Due to the

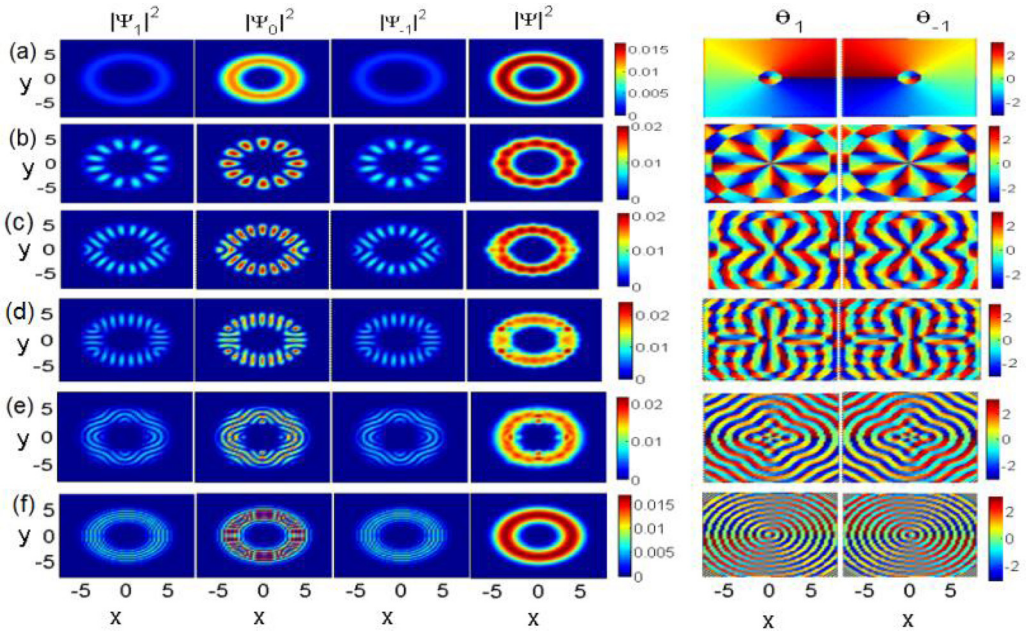

FIG. 2. Left panels: The ground-state density profiles of the $m_F = 1$ component, the $m_F = -1$ component, and the $m_F = 0$ component. Right panels: The phases of the $m_F = \pm 1$ components. The relative interaction strength $g = 5$ and the toroidal trap radius $r_0 = 4$. (a)–(f) The SOC strength is, respectively, taken as $\lambda = 0.25, 1.6, 2.4, 3, 4, 6.4$, which correspond to the phases of (A)–(F) in Fig. 1(a).

fact that the rotational and transitional symmetries are broken, the (B)–(D) phases have the periodic density modulation along the azimuthal direction. We take them as the first type of the stripe phase.

As the SOC and the relative interaction are further increased, the (E) phase emerges as the ground state, as shown in Figs. 1(a) and 1(c). The density and phase profiles of this phase are shown in Fig. 2(e). We find the density of this phase has the periodic density modulation along both the radial and the azimuthal directions, which realizes the second type of the stripe phase. This phase tends to be perpendicular to the hole with inward expansion.

Finally, we move to the case where both the SOC and the relative interaction are sufficiently strong, and the (F) phase emerges. Compared with the (E) phase, the periodic density modulation along the azimuthal direction disappears and along the radial direction becomes obvious. We take it as the third type of the stripe phase. This phase consists of alternating density domains along the radial direction, where stripes are filled and the three components are segregated, as shown in Fig. 2(f).

The properties of the six phases have been discussed for fixed toroidal trap radius $r_0 = 4$. When the SOC is weak, the (A) phase is preferred and the boundary of this phase is independent of the relative interaction. Due to the fact that the rotational and the transitional symmetry are broken, the (B)–(F) phases are classified as the three types of the stripe phases: the first type of the stripe phase [(B)–(D) phases] with the periodic density modulation along the azimuthal direction, the second type of the stripe phase [(E) phase] with the periodic density modulation along both the azimuthal and the radial directions, and the third type of the stripe phase [(F) phase] with the periodic density modulation along the radial direction. In all of these phases, the directions of the phase gradients of the $m_F = 1$ and $m_F = -1$ components are antisymmetric.

To get a deeper physical insight into this system, we study the ground-state phase diagrams without the quadratic Zeeman shift ($q = 0$) spanned by the SOC strength λ and the toroidal trap radius r_0 ($2 \leqslant r_0 \leqslant 6$) for fixed relative interaction g, as shown in Fig. 3. For the weak relative interaction ($g = 0.67$), four phases are shown in Fig. 3(a). The regimes of the (A) phase, the (C) phase, and the (D) phase decrease as r_0 is increased. The (C) phase is nonexistent for large toroidal trap radius r_0, which leads to the phase transforms from the (B) phase to the (D) phase directly. The toroidal trap radius plays an important role for the (B) phase for the weak relative interaction. The combination of the toroidal trap radius and the SOC makes the (B) phase occupy the largest regime, and the regime of the (B) phase increases as r_0 and g are

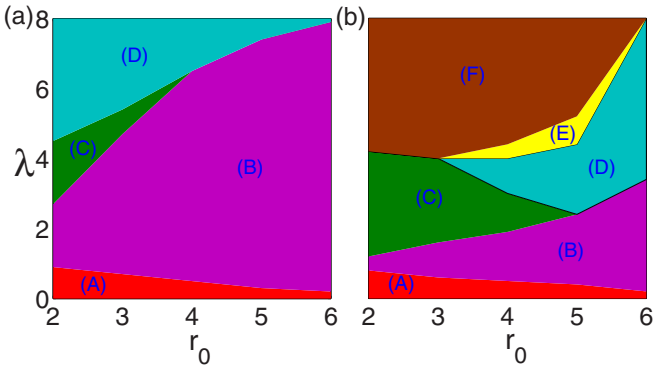

FIG. 3. The ground-state phase diagram spanned by the SOC strength λ and the toroidal trap radius r_0 without the quadratic Zeeman shift ($q = 0$). The relative interaction strength is (a) $g = 0.67$ and (b) $g = 5$, respectively.

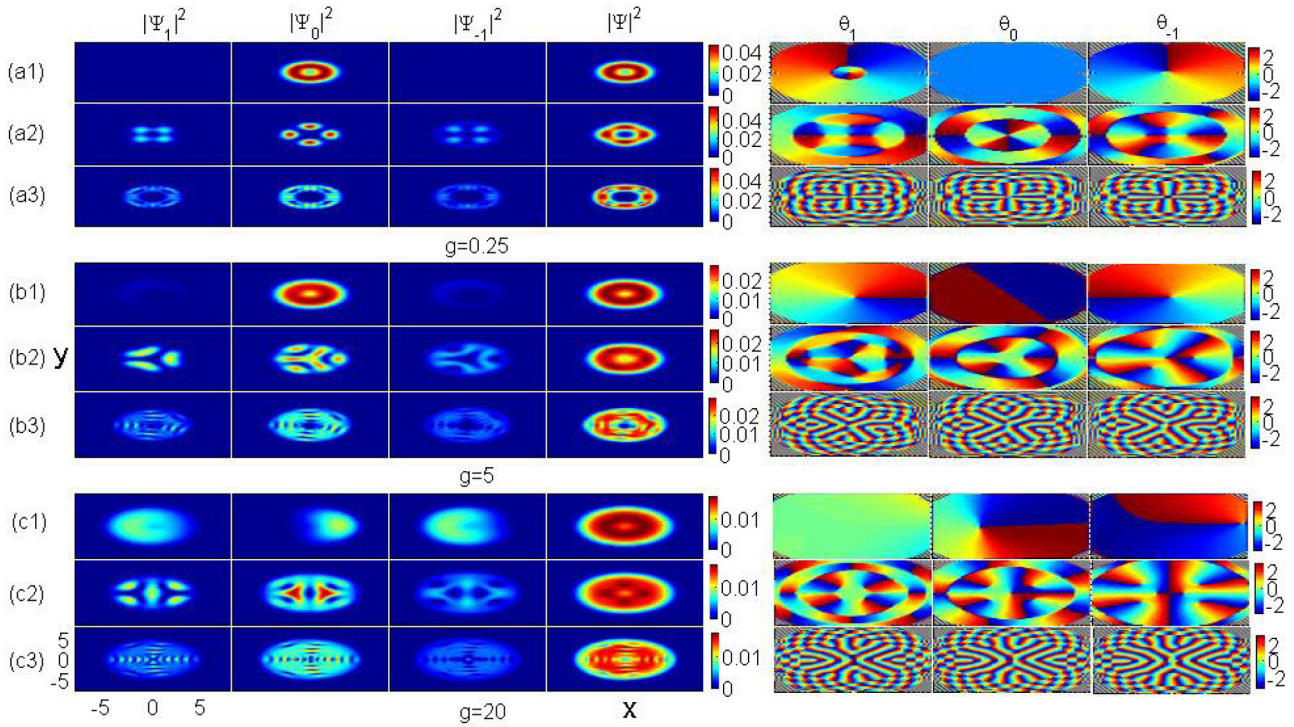

FIG. 4. The ground-state density and phase profiles for the $m_F = 1$, $m_F = 0$, and $m_F = -1$ component for the SOC strengths ($\eta 1$) $\lambda = 0.1$, ($\eta 2$) $\lambda = 1$, and ($\eta 3$) $\lambda = 4$ (η = a,b,c), respectively. The relative interaction strengths (al) $g = 0.25$, (bl) $g = 5$, and (cl) $g = 20$ (l = 1,2,3). The toroidal trap radius $r_0 = 2$ and the rotation frequency $\Omega = 0.1$.

increased. The phase diagram becomes richer when the relative interaction is strong ($g = 5$), where six phases are shown in Fig. 3(b). For the small toroidal trap radius r_0, the (D) phase in Fig. 3(a) is replaced by the (F) phase when the SOC strength λ is large. The region of the (F) phase also decreases with the toroidal trap radius r_0 increases. The (D) and (E) phases emerge near the toroidal trap radius $r_0 = 3$, and the regions of both phases get up to the largest for a certain value of r_0, respectively.

By comparing Figs. 3(a) and 3(b), we find that the relative interaction has little effect on the (A) phase. The system favors the (B) phase for the weak relative interaction. For both strong relative interaction and SOC, the (D) phase is replaced by the (F) phase. The (D) phase exists in both regions of the small toroidal trap radius with the weak relative interaction and the large toroidal trap radius with the strong relative interaction. The toroidal trap radius and the relative interaction play an important role for the (D) phase.

IV. THE GROUND-STATE PHASE STRUCTURES WITH THE ROTATION

We turn to study the ground-state phase structures of the rotational system. We take three typical rotational frequencies Ω, i.e., $\Omega = 0.1$, $\Omega = 0.25$, and $\Omega = 0.5$, and the toroidal trap radius is fixed as $r_0 = 2$.

Figure 4 displays the density and phase distributions of the ground-state phases with the low rotation frequency $\Omega = 0.1$. The SOC strengths are ($\eta 1$) $\lambda = 0.1$, ($\eta 2$) $\lambda = 1$, and ($\eta 3$) $\lambda = 4$, (η = a,b,c) and the relative interaction strengths are (al) $g = 0.25$, (bl) $g = 5$, and (cl) $g = 20$ (l = 1,2,3). For the weak SOC ($\lambda = 0.1$), the condensates mainly occupy the $m_F = 0$ component when the relative interaction $g = 0.25$ and $g = 5$. As the relative interaction grows ($g = 20$), the $m_F = 1$ and $m_F = -1$ components have nearly the same distributions of the density and occupy the left side around the toroidal trap. The $m_F = 0$ component occupies the right side around the toroidal trap, as depicted in Figs. 4($\eta 1$). For the relative interaction $g = 5$ and $g = 20$, Figs. 4(a2) and 4(a3) show that the densities of each component have the periodic density modulation along the azimuthal direction and the total densities also have the periodic density modulation with the weak SOC strength ($\lambda = 0.1$). With increase of the SOC, the system evolves from a triangular vortex [Fig. 4(b2)] into a pair of triangular vortices [Fig. 4(c2)]. For the large SOC strength ($\lambda = 4$), a series of vortices appears along the radial directions, which realizes a stripe phase with the periodic density modulation along the radial direction, as shown in Figs. 4(b3) and 4(c3).

Next, we study the density and phase distributions of the ground-state phases under the rotational frequency $\Omega = 0.25$. In Fig. 5, the parameter values of λ and g are the same as those in Fig. 4. When the SOC is relatively weak ($\lambda = 0.1$), the condensates mainly occupy the $m_F = 1$ and $m_F = -1$ components. With the increase of the relative interaction g, the densities of the three components exhibit obvious phase separation, as shown in Figs. 5(b1) and 5(c1). For the weak relative interaction $g = 0.25$ and large SOC $\lambda = 4$, the density of each component of the system forms a pentagon [Fig. 5(a3)]. There are four periodic density modulations along

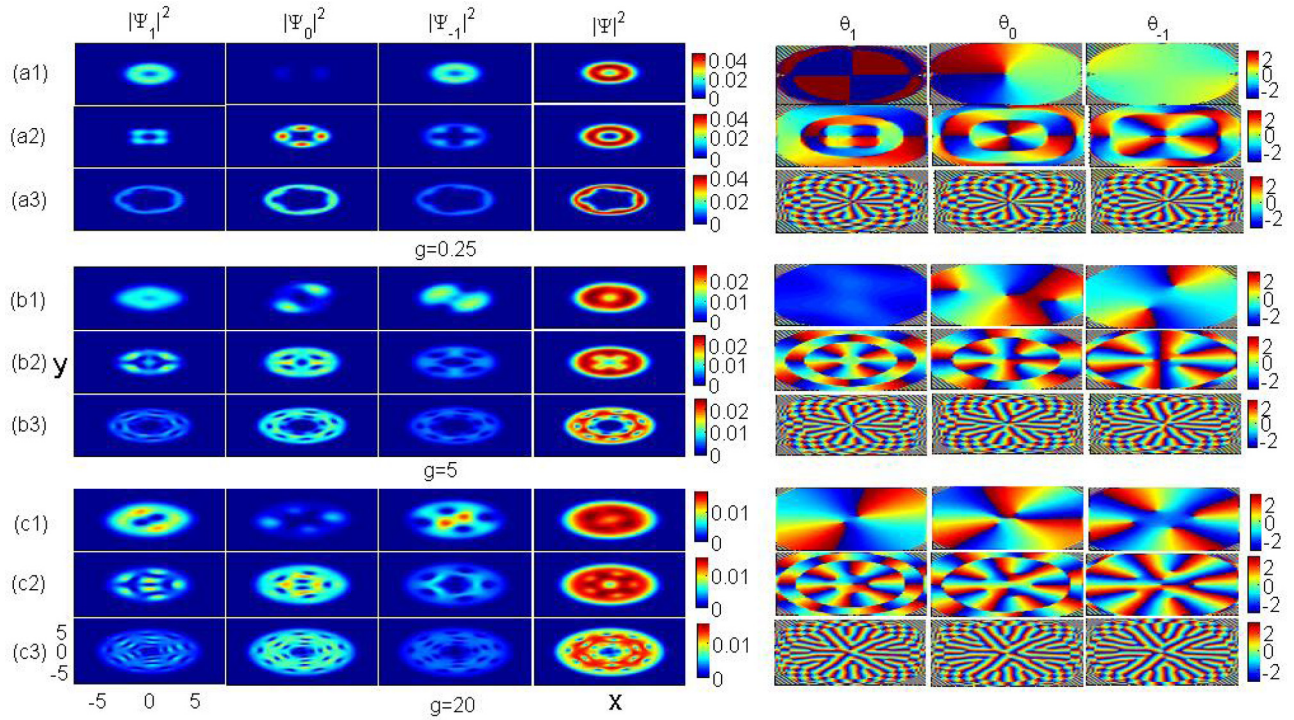

FIG. 5. The ground-state density and phase profiles for the $m_F = 1$, $m_F = 0$, and $m_F = -1$ components. The rotation frequency $\Omega = 0.25$ and other parameters are the same as in Fig. 4.

the azimuthal direction and the trap center region is pinned by zero quantized vortex in the $m_F = 1$ component and four vortices on the periphery of density profiles of the $m_F = 0$ and $m_F = 1$ components. The center region in the $m_F = 0$ component is pinned by a quantized vortex and in the $m_F = -1$ component is pinned by a doubly quantized vortex for $g = 5$ and $\lambda = 1$ [Fig. 5(b2)]. There are five periodic density modulations along the azimuthal direction and the middle region is a stripe phase in the $m_F = 1$ component. Five vortices locate on the periphery of density distributions and two vortices in the middle region in the $m_F = 1$ component. There is a large density hole in the $m_F = -1$ component in the trap center. The $m_F = 0$ component is pinned by a doubly quantized vortex and the $m_F = -1$ component is pinned by a triply quantized vortex when the relative interaction strength $g = 20$ and the SOC strength $\lambda = 1$ [Fig. 5(c2)]. For the large SOC strength $\lambda = 4$, each component forms a complex topological structure composed of a laminar vortex ring and a large density hole, where the number of laminar vortex ring is 2 at the relative interaction, as shown in Figs. 5(b3) and 5(c3), respectively.

Finally, Fig. 6 displays the density and phase distributions of the ground-state phases with the large rotational frequency $\Omega = 0.5$. For small relative interaction $g = 0.25$, it is the same as Fig. 5(a1) with $\lambda = 0.1$. With the increase of the SOC strength α, the densities of the three components form circles of the same radius. The winding number is $n - 1$ for the $m_F = 1$ component, n for the $m_F = 0$ component, and $n + 1$ for the $m_F = -1$ component (n is an integer), as shown in Figs. 6(a1)–6(a3). When the relative interaction increases ($g = 5$ and $g = 20$), we find the total density from the periodic density modulation along the azimuthal direction with the small SOC strength $\lambda = 0.1$ [Figs. 6(b1) and 6(c1)]. With the increase of the SOC strength ($\lambda = 1$ and $\lambda = 4$), each component also forms the laminar vortex ring.

From Fig. 4 to Fig. 6, we show the density and phase distributions of the ground-state phases of the system. When the relative interaction is weak and the SOC strength is small, the condensates occupy the $m_F = 0$ component for small rotational frequency. As the rotational frequency increases, the condensates occupy the $m_F = 1$ and $m_F = -1$ components. For the large SOC strength and small relative interaction, the total density of the system forms a stripe phase when the relative interaction is small. It forms a uniform ring when the rotation frequency becomes even faster. For the large SOC and strong relative interaction, the vortices tend to be elongated along the radius and linked one after another when the rotation frequency is small. It evolves from the the elongated effect of the vortices into a complex topological structure composed of a laminar vortex ring and a large density hole as the rotational frequency increases.

V. SUMMARY

We have investigated the ground-state structures of the spin-orbit-coupled spin-1 BEC in a 2D toroidal trap. For the system without the rotation, a rich variety of the ground-state phases is identified. For the fixed toroidal trap radius, the (A) phase is obtained with the weak SOC, and the relative interaction has little effect on this phase. The three types of stripe phases are identified due to the broken rotational and transitional symmetry: the first type of the stripe phase [(B)–(D) phases] with the periodic density modulation along the azimuthal direction, the second type of the stripe phase [(E) phase] with the periodic density modulation along both

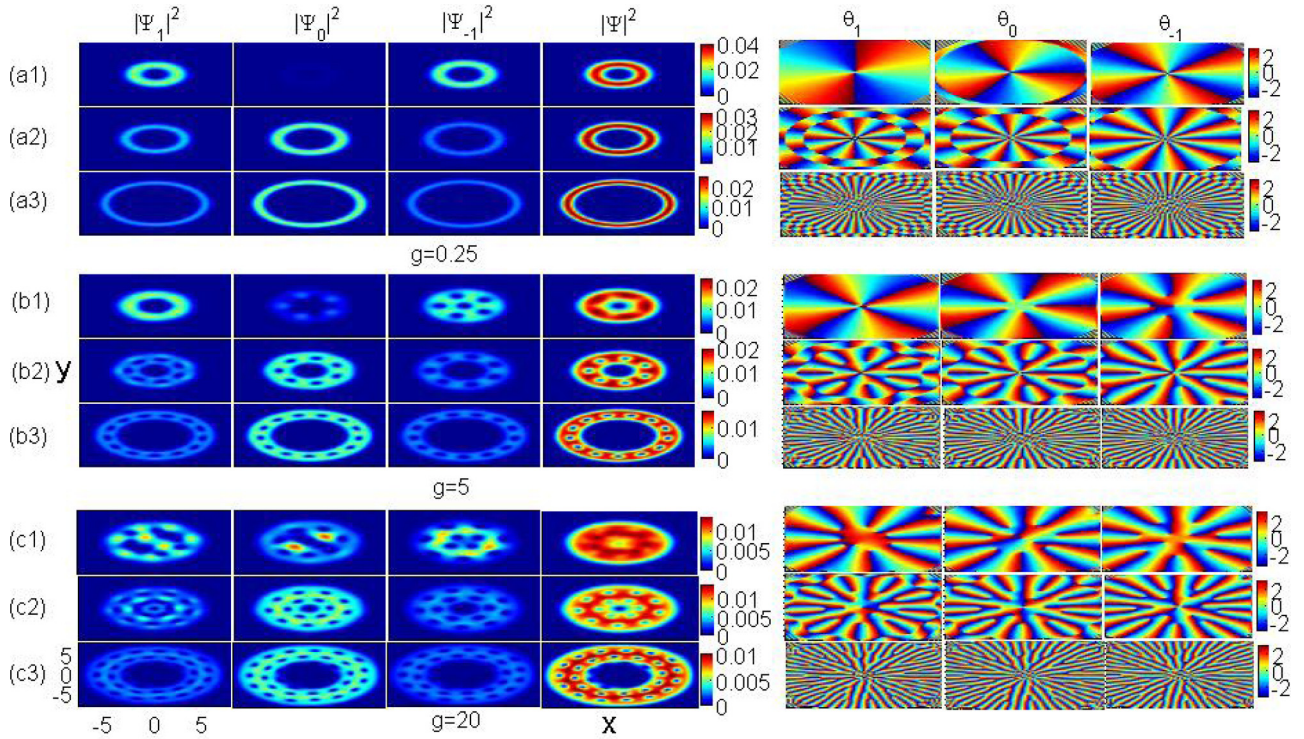

FIG. 6. The ground-state density and phase profiles for the $m_F = 1$, $m_F = 0$, and $m_F = -1$ components. The rotational frequency $\Omega = 0.5$ and other parameters are the same as in Fig. 4.

the azimuthal and the radial directions, and the third type of the stripe phase [(F) phase] with the periodic density modulation along the radial direction. The toroidal trap radius and the relative interaction play an important role for the (D) phase. By adding the rotation, the density of the system occupies the $m_F = 0$ component with the small rotation frequency and occupies both the $m_F = 1$ and $m_F = -1$ components with the large rotation frequency. For the strong relative interaction and SOC, the vortices are elongated along the radius and linked one after another. When the rotational frequency increases, the density evolves from the the elongated effect of the vortices into a laminar vortex ring.

ACKNOWLEDGMENTS

This work is supported by the NSF of China under Grant No. 11374036 and the National Basic Research Program of China under Grant No. 2012CB821403.

[1] I. Žutić, J. Fabian, and S. Das Sarma, Rev. Mod. Phys. **76**, 323 (2004).
[2] J. Wunderlich, B. Kaestner, J. Sinova, and T. Jungwirth, Phys. Rev. Lett. **94**, 047204 (2005).
[3] S. Murakami, Phys. Rev. Lett. **97**, 236805 (2006).
[4] M. Z. Hasan and C. L. Kane, Rev. Mod. Phys. **82**, 3045 (2010).
[5] X. L. Qi and S. C. Zhang, Rev. Mod. Phys. **83**, 1057 (2011).
[6] Y. J. Lin, K. Jiménez-García, and I. B. Spielman, Nature (London) **471**, 83 (2011).
[7] J. Y. Zhang, S. C. Ji, Z. Chen, L. Zhang, Z. D. Du, B. Yan, G. S. Pan, B. Zhao, Y. J. Deng, H. Zhai, S. Chen, and J. W. Pan, Phys. Rev. Lett. **109**, 115301 (2012).
[8] L. W. Cheuk, A. T. Sommer, Z. Hadzibabic, T. Yefsah, W. S. Bakr, and M. W. Zwierlein, Phys. Rev. Lett. **109**, 095302 (2012).
[9] C. Qu, C. Hamner, M. Gong, C. W. Zhang, and P. Engels, Phys. Rev. A **88**, 021604(R) (2013).
[10] Z. Wu, L. Zhang, W. Sun, X. T. Xu, B. Z. Wang, S. C. Ji, Y. Deng, S. Chen, X. J. Liu, and J. W. Pan, Science **354**, 83 (2016).
[11] L. Huang, Z. Meng, P. Wang, P. Peng, S. L. Zhang, L. Chen, D. Li, Q. Zhou, and J. Zhang, Nat. Phys. **12**, 540 (2016).
[12] C. Wang, C. Gao, C. M. Jian, and H. Zhai, Phys. Rev. Lett. **105**, 160403 (2010).
[13] T. L. Ho and S. Zhang, Phys. Rev. Lett. **107**, 150403 (2011).
[14] C.-J. Wu, I. Mondragon-Shem, and X.-F. Zhou, Chin. Phys. Lett. **28**, 097102 (2011).
[15] H. Hu, B. Ramachandhran, H. Pu, and X.-J. Liu, Phys. Rev. Lett. **108**, 010402 (2012).
[16] R. M. Wilson, B. M. Anderson, and C. W. Clark, Phys. Rev. Lett. **111**, 185303 (2013).
[17] X. Chen, M. Rabinovic, B. M. Anderson, and L. Santos, Phys. Rev. A **90**, 043632 (2014).
[18] M. Gong, G. Chen, S.-T. Jia, and C. W. Zhang, Phys. Rev. Lett. **109**, 105302 (2012).
[19] J. Radić, T. A. Sedrakyan, I. B. Spielman, and V. Galitski, Phys. Rev. A **84**, 063604 (2011).
[20] X. F. Zhou, J. Zhou, and C. Wu, Phys. Rev. A **84**, 063624 (2011).
[21] X. Q. Xu and J. H. Han, Phys. Rev. Lett. **107**, 200401 (2011).

[22] C. F. Liu and W. M. Liu, Phys. Rev. A **86**, 033602 (2012).
[23] C. F. Liu, H. Fan, Y. C. Zhang, D. S. Wang, and W. M. Liu, Phys. Rev. A **86**, 053616 (2012).
[24] J. Ruseckas, G. Juzeliūnas, P. Öhberg, and M. Fleischhauer, Phys. Rev. Lett. **95**, 010404 (2005).
[25] G. Juzeliūnas, J. Ruseckas, M. Lindberg, L. Santos, and P. Öhberg, Phys. Rev. A **77**, 011802(R) (2008).
[26] G. Jūzeliunas, J. Ruseckas, and J. Dalibard, Phys. Rev. A **81**, 053403 (2010).
[27] D. L. Campbell, G. Juzeliūnas, and I. B. Spielman, Phys. Rev. A **84**, 025602 (2011).
[28] X. J. Liu, K. T. Law, and T. K. Ng, Phys. Rev. Lett. **112**, 086401 (2014).
[29] Z. F. Xu, L. You, and M. Ueda, Phys. Rev. A **87**, 063634 (2013).
[30] B. M. Anderson, I. B. Spielman, and G. Juzeliūnas, Phys. Rev. Lett. **111**, 125301 (2013).
[31] D. L. Campbell, R. M. Price, A. Putra, A. Valdés-Curíel, D. Trypogeorgos, and I. B. Spielman, Nat. Commun. **7**, 10897 (2016).
[32] X. Luo, L. Wu, J. Chen, Q. Guan, K. Gao, Z.-F. Xu, L. You, and R. Wang, Sci. Rep. **6**, 18983 (2016).
[33] K. Sun, C. Qu, Y. Xu, Y. Zhang, and C. Zhang, Phys. Rev. A **93**, 023615 (2016).
[34] W. Han, X. F. Zhang, S. W. Song, H. Saito, W. Zhang, W. M. Liu, and S. G. Zhang, Phys. Rev. A **94**, 033629 (2016).
[35] Z. Q. Yu, Phys. Rev. A **93**, 033648 (2016).
[36] M. Kato, X. F. Zhang, D. Sasaki, and H. Saito, Phys. Rev. A **94**, 043633 (2016).
[37] G. I. Martone, F. V. Pepe, P. Facchi, S. Pascazio, and S. Stringari, Phys. Rev. Lett. **117**, 125301 (2016).
[38] X. Y. Huang, F. X. Sun, W. Zhang, Q. Y. He, and C. P. Sun, Phys. Rev. A **95**, 013605 (2017).
[39] C. Ryu, M. F. Andersen, P. Cladé, V. Natarajan, K. Helmerson, and W. D. Phillips, Phys. Rev. Lett. **99**, 260401 (2007).
[40] S. Beattie, S. Moulder, R. J. Fletcher, and Z. Hadzibabic, Phys. Rev. Lett. **110**, 025301 (2013).
[41] A. I. Yakimenko, K. O. Isaieva, S. I. Vilchinskii, and M. Weyrauch, Phys. Rev. A **88**, 051602(R) (2013).
[42] Y. Li, W. Pang, and B. A. Malomed, Phys. Rev. A **86**, 023832 (2012).
[43] P. Mason and N. G. Berloff, Phys. Rev. A **79**, 043620 (2009).
[44] X. F. Zhang, M. Kato, W. Han, S. G. Zhang, and H. Saito, Phys. Rev. A **95**, 033620 (2017).
[45] H. Wang, L. H. Wen, H. Yang, C. X. Shi, and J. H. Li, J. Phys. B **50**, 155301 (2017).
[46] A. C. White, Y. P. Zhang, and T. Busch, Phys. Rev. A **95**, 041604(R) (2017).
[47] F. E. Meijer, A. F. Morpurgo, and T. M. Klapwijk, Phys. Rev. B **66**, 033107 (2002).